Journal of ELECTRONIC MATERIALS, Vol. 48, No. 5, 2019
https://doi.org/10.1007/s11664-019-07056-2

Photocatalytic Degradation of Methylene Blue (MB) over α-Fe_2O_3 Nanospindles Prepared by a Hydrothermal Route

XUAN HOA VU,[1] LUONG HUU PHUOC,[2] NGUYEN DAC DIEN,[3,6] THI THU HA PHAM,[4] and LUONG DUY THANH[5]

1.—Faculty of Physics and Technology, Thai Nguyen University of Science, Tan Thinh Ward, Thai Nguyen City, Vietnam. 2.—School of Engineering Physics, Hanoi University of Science and Technology, No. 1 Dai Co Viet Road, Hai Ba Trung District, Hanoi, Vietnam. 3.—Faculty of Labour Protection, Vietnam Trade Union University, No. 169 Tay Son Street, Dong Da District, Hanoi, Vietnam. 4.—Faculty of Chemistry, Thai Nguyen University of Science, Tan Thinh Ward, Thai Nguyen City, Vietnam. 5.—Thuyloi University, 175 Tay Son, Dong Da, Hanoi, Vietnam. 6.—e-mail: diennd@dhcd.edu.vn

Well-crystalline iron oxide (α-Fe_2O_3) nanospindles have been prepared using a simple hydrothermal process at temperature of 240°C for different durations (24 h, 36 h, 48 h, and 60 h). The products were characterized by x-ray diffraction analysis, scanning electron microscopy, transmission electron microscopy, energy-dispersive x-ray spectroscopy, and visible absorption measurements. Detailed characterization of their structure and composition confirmed formation of pure α-Fe_2O_3 with rhombohedral crystal structure. The photocatalytic activity of the obtained α-Fe_2O_3 for demineralization of methylene blue (MB) in aqueous solution under ultraviolet (UV) light irradiation was evaluated. Ultraviolet–visible (UV–Vis) spectroscopy indicated a decrease in the absorbance intensity and concentration of the dye. Mechanistic investigation revealed that ·OH and ·O radicals played a crucial role in the degradation process of methylene blue. The α-Fe_2O_3 nanospindles presented high photocatalytic activity towards MB with degradation efficiency of 78% within 6 h of irradiation. These results demonstrate that α-Fe_2O_3 nanospindles are suitable for treatment of wastewater.

Key words: α-Fe_2O_3 nanospindles, photocatalytic degradation, methylene blue, hydrothermal treatment

INTRODUCTION

Environmental problems are mostly caused by disposal of waste and pollutants that are toxic to human health without proper treatment. In recent years, the photocatalytic technique has attracted significant interest for decreasing the concentration of dyes in wastewater before discharge into the environment. This method is capable, efficient, environmentally friendly, economical, and simple, offering complete degradation of dyes such as methylene blue (MB) used in textile industries, including the dyeing and printing industries. The photocatalytic technique does not produce secondary waste products that require further processing. Recently, there has been widespread interest in synthesis of semiconductor metal-oxide photocatalysts such as zinc oxide (Co-doped ZnO,[1] graphene oxide/ZnO hybrid[2]), titanium oxide (TiO_2[3]), α-Fe_2O_3/graphene oxide,[4] graphene oxide/BiOBr,[5] TiO_2/ZrO_2 composite,[6] etc. for degradation of a variety of organic pollutants under irradiation by light of different wavelengths. Among photocatalytic materials, α-Fe_2O_3 is an effective photocatalyst due to its exceptional properties, such as high chemical stability, high catalytic activity, low-cost synthesis, biofriendly nature, and high resistance to corrosion.[4] Hematite (α-Fe_2O_3) is an n-type

(Received October 18, 2018; accepted February 8, 2019; published online February 21, 2019)

semiconductor (bandgap E_g = 2.1 eV[7]) that is widely used in various applications, e.g., sensors,[8] optoelectronics,[9] antibacterial treatment,[10] energy storage in lithium rechargeable batteries,[11,12] magnetic recording media and magnetic devices,[13] heavy-metal removal in water treatment applications,[12,14] biomedical applications,[15] and so on. Because of its high electrical conductivity, sensitivity, and large surface area, iron oxide nanomaterials with different shapes such as nanoflowers,[11] nanorods,[16] nanoparticles,[7] nanodisks,[17] spindles,[18] and hollow spheres[14] have been fabricated by various methods, including solvothermal,[4,19] hydrothermal,[17,18] and microwave-assisted methods[14] for application as photocatalysts with high photocatalytic performance under UV irradiation. Additionally, their high adsorption rate and light absorptivity lead to efficient charge transport in the photocatalyst. The focus of this work is synthesis of α-Fe_2O_3 nanospindles with orthorhombic structure using a hydrothermal method and their potential photocatalytic activity for removal of methylene blue (MB) dye molecules under UV light irradiation. The mechanisms behind the observed results are then discussed in detail. The nanospindles were characterized in terms of their morphological, structural, compositional, and photocatalytic properties using various experimental techniques. Besides, we also highlight the promising applications of α-Fe_2O_3 nanospindles for elimination of pollution.

EXPERIMENTAL PROCEDURES

All reagents were of analytical grade and used as received without further purification. Ferric chloride hexahydrate ($FeCl_3{\cdot}6H_2O$) was taken as precursor salt for Fe_2O_3, and sodium dihydrogen phosphate (NaH_2PO_4) was used as precipitating reagent. All chemicals were purchased from Merck (Germany). Double-distilled water (DDW) was used throughout the experiments. The synthesis process is described as follows: First, 0.5 g $FeCl_3{\cdot}6H_2O$ was dissolved in 50 ml deionized water under magnetic stirring to form $FeCl_3$ solution. Likewise, 0.012 g NaH_2PO_4 powder was separately dissolved in 50 ml distilled water using a magnetic stirrer to obtain NaH_2PO_4 solution. Then, NaH_2PO_4 solution was dropped slowly into $FeCl_3$ solution under continuous stirring for 30 min at room temperature to form a transparent system and complete the reaction. After that, the homogeneous mixture was transferred into a 100-ml Teflon-lined stainless-steel autoclave and heated at temperature of 240°C for 24 h, 36 h, 48 h, or 60 h. After reaction completion, the autoclave was allowed to attain room temperature. The red-colored precipitate was collected by filtration, repeatedly rinsed with ethanol followed by DDW, and finally dried at 80°C for 24 h in a hot air oven. The synthesized material was used as photocatalyst for photodegradation of methylene blue.

The crystal structure of the obtained samples was characterized by x-ray diffraction (XRD) analysis (D8 Advance; Bruker, Germany) using Cu K_α radiation (wavelength λ = 1.5406 Å) in the 2θ angle range of 10° to 70° at rate of 3°/min. The morphology and microstructure of the samples were examined by field-emission scanning electron microscopy (FESEM, Hitachi S4800, Japan) at accelerating voltage of 10 kV. Transmission electron microscopy (TEM) images were obtained using a Philips CM-200 operated at 80 kV. The elemental composition of the synthesized samples was analyzed by energy-dispersive x-ray spectroscopy (EDS, Oxford JEOL 5410 LV, Japan) operating at 15 kV.

The photocatalytic activity of the obtained α-Fe_2O_3 samples was investigated in photodegradation of methylene blue (MB) under UV light irradiation at room temperature. Before the irradiation process, 50 mg α-Fe_2O_3 powder was dispersed in 100 ml aqueous solution of methylene blue (MB) dye with initial concentration C_0 = 10 mg/l, and the mixture was magnetically stirred in the dark for 30 min to establish adsorption–desorption equilibrium. After stirring, the solution was exposed to UV light (λ = 365 nm) using a 125-W mercury lamp as the light source at 25 cm away from the liquid level of the MB aqueous solution. After each 1-h interval, aliquots were withdrawn from the mixture solution and the MB concentration analyzed by UV–Vis spectrophotometry in in the wavelength range of 400 nm to 800 nm. The concentration C of the treated dye was determined by measuring the absorbance of the solution by UV–Vis absorption spectroscopy (Shimadzu UV-1800) in the range of 400 nm to 800 nm to calculate the degradation efficiency. The rate of degradation for the decomposition of MB (decrease in absorption intensity versus irradiation time) was estimated by evaluating the change in absorbance in the observed UV–Vis spectra.

RESULTS AND DISCUSSION

When NaH_2PO_4 was added into $FeCl_3$ solution, $Fe(OH)_3$ precipitate formed as follows:

$$FeCl_3 + NaH_2PO_3 + 3H_2O \rightarrow Fe(OH)_3 + NaCl + H_3PO_4 + 2HCl \quad (1)$$

During the hydrothermal process, $Fe(OH)_3$ was transferred into the intermediate phase FeOOH then terminated as Fe_2O_3 according to the following reactions:

$$Fe(OH)_3 \rightarrow \beta\text{-}FeOOH + H_2O \quad (2)$$

$$2\beta\text{-}FeOOH \rightarrow \alpha\text{-}Fe_2O_3 + H_2O \quad (3)$$

The reactions were conducted in a sealed autoclave, where the phase transformation reaction

proceeded under the self-generated pressure. A possible mechanism for the nanospindle formation is proposed as follows: First, α-Fe_2O_3 molecules crystallize to form nanoparticles, then self-assembled into nanospindles.

Figure 1a–d shows the characterization results for the iron oxide (α-Fe_2O_3) product obtained at hydrothermal temperature of 240°C for 48 h. Figure 1a reveals relatively uniform spindle-like particles with narrow size distribution; most the of spindles are 150 nm to 200 nm in length and about 75 nm in diameter. The spindles have a relatively rough surface and consist of smaller nanoparticles approximately 10 nm in size. The corresponding TEM image (Fig. 1b) indicates that they had solid structure, because of the lack of contrast between the edge and center of the spindle. The preferential growth direction of spindle hematite is [001], called the revolution axis. Oriented attachment of nanocrystals along the [211] zone axis is the main reason for the spindle-shape structure.[20]

The elemental composition of synthesized nanospindles was examined by energy-dispersive spectroscopy (Fig. 1c). The typical EDS spectrum of α-Fe_2O_3 obtained by hydrothermal treatment at 240°C for 48 h shows well-defined peaks for iron (Fe) and oxygen (O) corresponding to the composition of iron oxide with atomic ratio of Fe to O of 1:1.7, in good agreement with the stoichiometry of Fe_2O_3. Additionally, no peaks corresponding to other elements were observed in the spectrum, confirming the highly pure state of the prepared hematite.

The crystalline structure of the α-Fe_2O_3 nanospindles obtained by treatment for 48 h with corresponding 2θ values and crystalline planes are shown by the XRD pattern in Fig. 1d. The sharp peaks confirm that the product is well crystallized in nature, matching well with the standard pattern for pure hematite phase α-Fe_2O_3 in Joint Committee on Powder Diffraction Standards (JCPDS) card no. 33-0664 with rhombohedral structure and primitive cell space group *R3c*. According to the interplanar spacing of (113) and (110) planes, the lattice constants were calculated as approximately $a = b = 0.50356$ nm, $c = 1.37489$ nm, $\alpha = \beta = 90°$, and $\gamma = 120°$. Except for those corresponding to the rhombohedral α-Fe_2O_3 structure, no other diffraction reflections were seen in the pattern, revealing that the synthesized product was pure α-Fe_2O_3. The perceptible broadening of the characteristic diffraction peaks indicates nanosized crystalline domains. The mean crystalline size was estimated from the

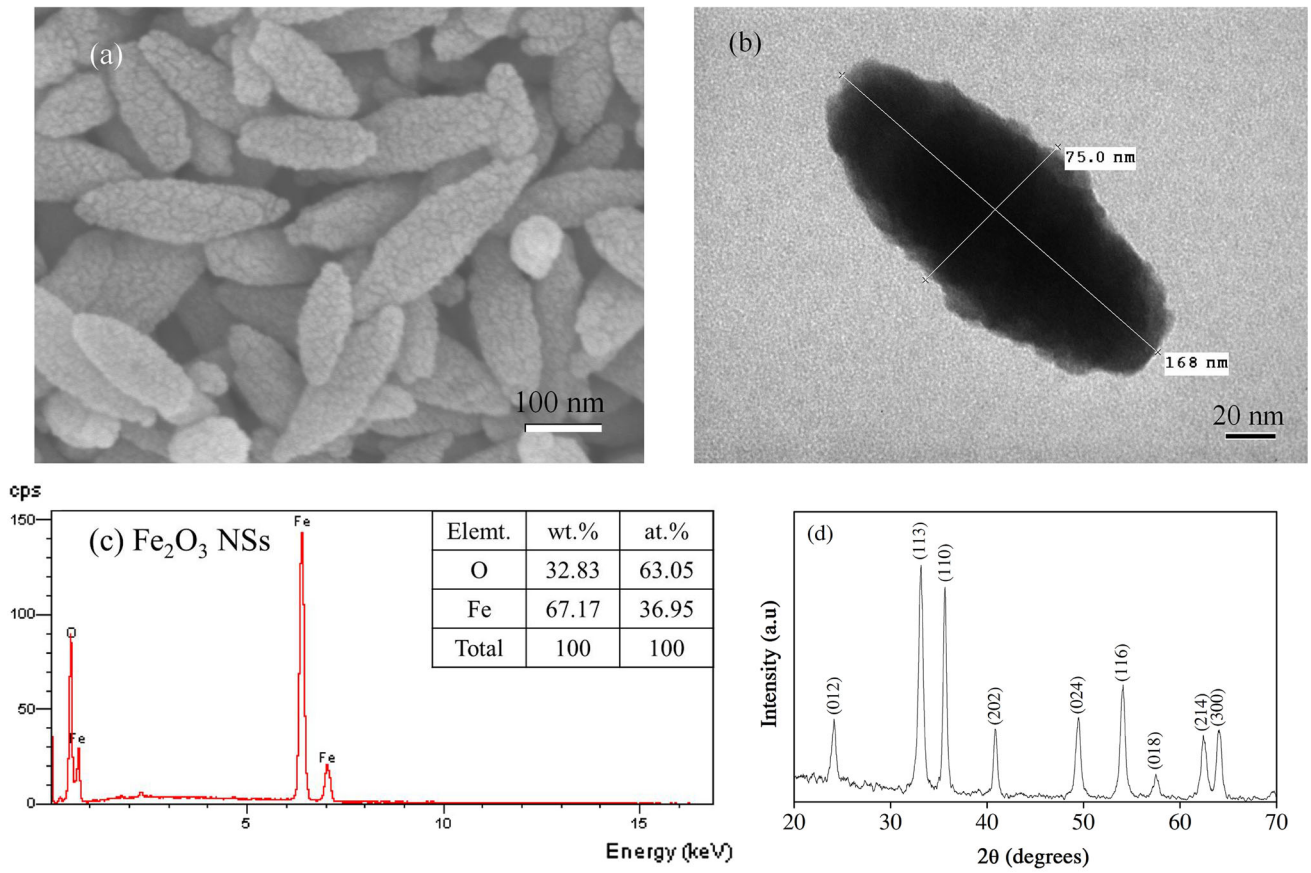

Fig. 1. FESEM (a), TEM image (b), EDS spectrum (c), and XRD pattern (d) of spindle-like hematite prepared by hydrothermal processing at 240°C for 48 h.

main reflection peak (113) at $2\theta = 33.14^\circ$ using the Debye–Scherrer formula[1]:

$$D = \frac{k\lambda}{B\cos\theta}, \quad (4)$$

where D is the crystalline size, λ is the x-ray wavelength, k is the shape factor or Scherrer constant (k = 0.94), B (rad) is the full-width at half-maximum (FWHM), and θ is the diffraction angle. The crystalline size was calculated as approximately 33 nm using the values $\lambda = 0.15406$ nm, $B = 0.27^\circ$, and $\theta = 16.57^\circ$. This result is inconsistent with the FESEM image, because the major morphology of the nanocrystals is not completely spherical. The lack of other peaks in the spectrum shows that the synthesized sample was phase pure. Even though sodium chloride (NaCl) is a byproduct in the reaction solution, no diffraction peaks for NaCl were observed by XRD due to the small amount of residual NaCl in the as-prepared α-Fe_2O_3 sample.

Figure 2a–c shows FESEM images of α-Fe_2O_3 products prepared by hydrothermal treatment at 240°C for different durations of 24 h, 36 h, and 60 h, respectively. When the reaction time differed from 48 h, the size distribution also became wider. The obtained products show a series of distinct structures: nanospindles, amorphous nanoparticles, and pseudospheres. Variation of the reaction time did not influence the morphology but evidently changed the size distribution of the α-Fe_2O_3 nanospindles. When the reaction time was 24 h, the initial product emerged as pseudospherical α-Fe_2O_3 particles with diameter of about 50 nm to 75 nm (Fig. 2a). When the reaction time was prolonged to 36 h, short spindles grew out of these pseudospherical particles, indicating the occurrence of self-assembly (Fig. 2b). The length and width of these spindles were about 100 nm to 150 nm and 50 nm to 70 nm, respectively. When the reaction time was increased to 60 h, the spindles coarsened and became nonuniform in structure (Fig. 2c). It is expected that globular shape would be unfavorable in terms of the photodegradation performance.[17]

Methylene blue (MB), a common organic pollutant resulting from industrial production of dyes, was adopted in this study to evaluate the photocatalytic activity of the synthesized α-Fe_2O_3 samples. To examine the activity of α-Fe_2O_3 in the degradation of MB, we carried out a blank experiment, i.e., without addition of α-Fe_2O_3 photocatalyst; No significant degradation was observed, even though the sample was exposed to UV illumination (Fig. 3a), revealing that MB is very stable in aqueous medium under ultraviolet light in the absence of α-Fe_2O_3. However, when α-Fe_2O_3 nanospindles were present in the solution under UV illumination, the intensity of the main absorbance peak of MB at 665 nm decreased over time, revealing that the α-Fe_2O_3 catalyst could effectively degrade MB dye molecules. It is expected that nanospindles prepared using different durations will possess slightly different morphologies.[20] Therefore, it is anticipated that the different photocatalytic activities of the

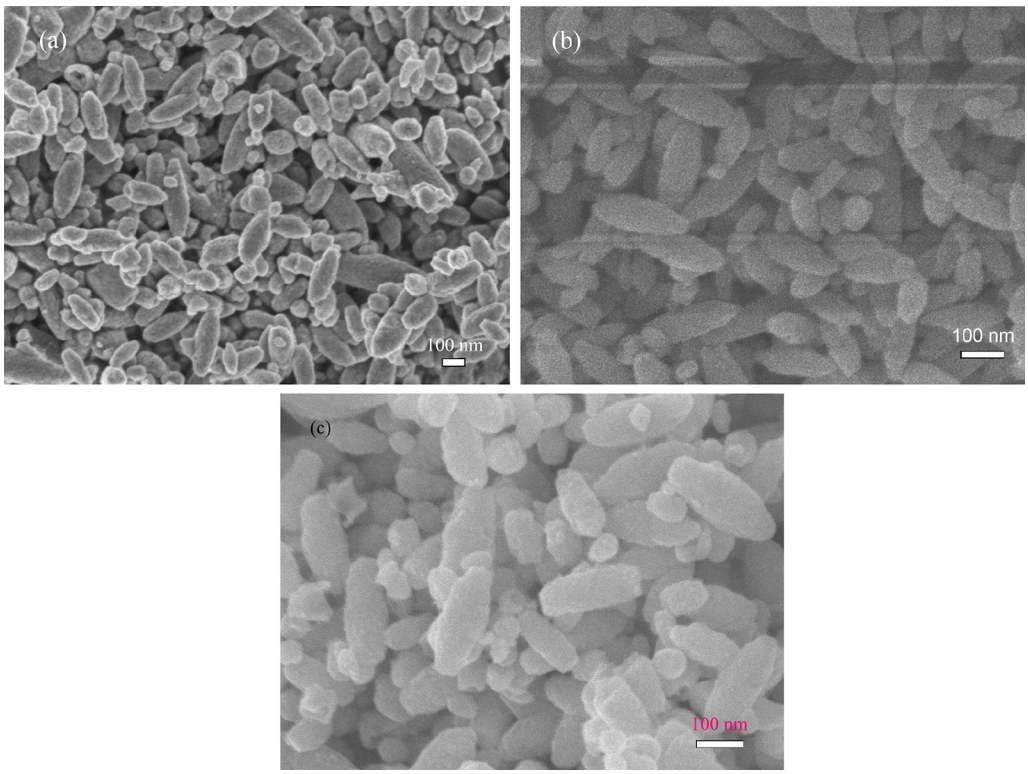

Fig. 2. FESEM images of α-Fe_2O_3 prepared by hydrothermal processing at 240°C for 24 h (a), 36 h (b), and 60 h (c).

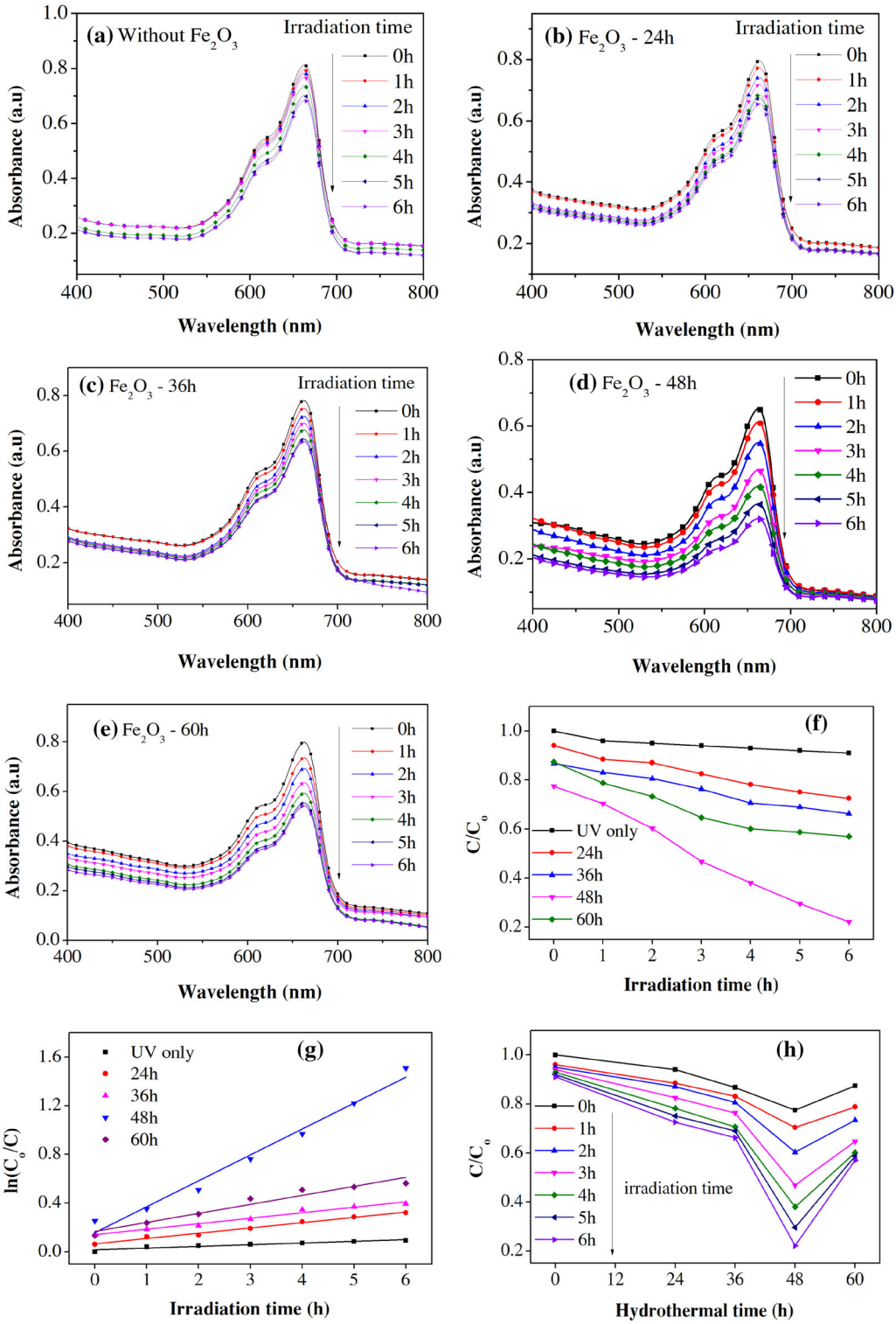

Fig. 3. Absorption spectra during MB dye degradation without photocatalyst (a) and with α-Fe_2O_3 nanospindles prepared through hydrothermal method at 240°C for 24 h (b), 36 h (c), 48 h (d), and 60 h (e) as photocatalyst under ultraviolet (UV) light irradiation (λ = 365 nm) for different irradiation times (0 h to 6 h); (f) the decrease of MB concentration with respect to time without and with α-Fe_2O_3 prepared by hydrothermal processing for different durations, (g) pseudo-first-order kinetic plot between $\ln(C_0/C)$ and irradiation time; (h) plot between C/C_0 and hydrothermal time at different irradiation times, where zero hydrothermal time means without photocatalyst.

samples synthesized with different durations will vary because the absorption and electron transfer strongly depend on the surface structure of the nanocrystal.[17] Figure 3b–e shows the photocatalytic efficiency and reaction constant of the α-Fe_2O_3 nanospindle samples obtained by hydrothermal

processing for various durations, after exposure to UV irradiation at regular time intervals (0 h to 6 h). The degradation efficiency is defined as C/C_0, where C_0 and C are the initial and postirradiation concentrations of MB at a specific time, respectively.[17] Figure 3f shows the concentration change C/C_0 versus time for photodegradation of MB without and with α-Fe_2O_3 obtained by hydrothermal processing with different durations. The maximum MB removal capacity for the noncatalyst sample reached only 9% after UV irradiation for 6 h. However, the MB removal capacity reached about 27% after 6 h when using the α-Fe_2O_3 treated for 24 h as photocatalyst. The irradiation time and hydrothermal time are crucial factors that influence the photocatalytic activity of α-Fe_2O_3. It was found that, among the four samples, the α-Fe_2O_3 nanospindles synthesized for 48 h showed superior photocatalytic activity; the MB degradation efficiency could reach about 78% for this sample after 6 h of UV irradiation, while the efficiency for the samples synthesized for 36 h and 60 h was 34% and 43%, respectively. It is reasonable to attribute that this high photocatalytic activity of the α-Fe_2O_3 sample synthesized for 48 h to its high specific surface area, good crystallinity, and uniform morphology. Another key factor contributing to this enhanced photocatalytic activity for MB degradation is adsorption of MB on nanostructured α-Fe_2O_3. The adsorption performance of the nanostructures is greatly improved by enlarging the surface area. As mentioned in previous work,[17] the occurrence of aggregation during annealing treatment results in a decrease in active reaction sites and the photocatalytic activity of the annealed sample. Consequently, we used the as-synthesized α-Fe_2O_3 product without annealing treatment to investigate its degradation performance.

The photocatalytic degradation of MB follows the pseudo-first-order kinetic model[6]:

$$-\ln\frac{C}{C_0} = \kappa t, \tag{5}$$

where κ is the first-order kinetic constant, C_0 is the initial concentration of MB, and C is the residual concentration at irradiation time t. The kinetic reaction rate can be calculated as[1]

$$R = -\frac{\mathrm{d}C}{\mathrm{d}t} = \frac{\kappa KC}{1+KC}, \tag{6}$$

where K is the adsorption constant of MB on the photocatalyst. When the concentration of MB becomes very low ($KC \ll 1$),

$$\ln\frac{C_o}{C} \approx \kappa Kt = K_{obs}t, \tag{7}$$

where K_{obs} is the observed rate constant of the photodegradation reaction.

Figure 3g shows the dependence of $\ln(C_0/C)$ on the irradiation time for MB solution in both cases, i.e., absence and presence of catalyst. It is seen that the degradation rate of MB increases with increasing hydrothermal processing time. Additionally, the results show that the α-Fe_2O_3 treated for 48 h showed the greatest ability to mineralize the dye. The reaction rate constant κ was calculated according to Eq. 5. The calculated results show that the α-Fe_2O_3 nanospindles treated for 48 h showed the highest reaction rate constant of $0.21\,h^{-1}$. For comparison, the values of the constant κ corresponding to α-Fe_2O_3 nanospindles treated for 24 h, 36 h, and 60 h were $0.04\,h^{-1}$, $0.04\,h^{-1}$, and $0.07\,h^{-1}$, respectively. It is evident that the photocatalytic performance of α-Fe_2O_3 nanospindles is comparable to that of α-Fe_2O_3 nanodisks.[21] The surface area is the principal parameter affecting the catalytic efficiency of iron oxides in degradation of MB. The morphology of the α-Fe_2O_3 nanodisks consists of dense disk-like agglomerates. Consequently, the interparticle spaces in the aggregate are small.[22] The reason why the α-Fe_2O_3 sample treated for 48 h showed the most effective degradation is its high adsorption rate. Use of a proper hydrothermal treatment duration for α-Fe_2O_3 facilitates the photocatalytic pathway and enhances the charge-transfer efficiency, resulting in effective degradation of MB. The enhanced photocatalytic activity results from a decrease in the recombination rate and a higher adsorption rate due to the hydrothermal treatment.

Detailed results regarding the ratio of the methylene blue (MB) concentration before and after irradiation with UV light are summarized in Table - I, revealing that all four samples showed photocatalytic behavior, with the Fe_2O_3 sample treated for 48 h being the most effective. The C/C_0 ratios for the four α-Fe_2O_3 samples synthesized for 48 h, 24 h, 36 h, and 60 h after UV irradiation for 6 h were 0.22, 0.72, 0.66, and 0.56, respectively. The better performance of the Fe_2O_3 sample treated for 48 h can be attributed to its highly porous structure and high surface area.

The photocatalytic reaction only involves a surface charge-transfer process.[17] Under UV irradiation, α-Fe_2O_3 absorbs the photon energy to form a hole and electron (Eq. 8), which participate in the photooxidation process on the surface of the catalyst. Holes can combine with water to form highly reactive hydroxide radicals (·OH) (Eq. 9), which are found to be the main active species in the degradation system.[22] Photogenerated electrons can be captured by dissolved oxygen in the dye solution to form peroxide radicals or superoxide radical anions ($\cdot O_2^-$) (Eq. 10). ·OH and $\cdot O_2^-$ are usually reported to be the probable oxidizing agents with the ability to fragment dye molecules directly by reacting with MB to form CO_2 and H_2O as degradation products (Eqs. 11 and 12).[5]

$$\alpha\text{-}Fe_2O_3 + h\nu \rightarrow \alpha\text{-}Fe_2O + h^+_{VB} + e^-_{CB} \tag{8}$$

Table I. Dependence of C/C_0 ratio on UV irradiation time for different α-Fe_2O_3 samples

Time (h)	UV Only	24 h	36 h	48 h	60 h
0	1.00	0.94046	0.86729	0.77464	0.87403
1	0.96	0.88466	0.83082	0.70363	0.78796
2	0.95	0.87045	0.80599	0.60251	0.73311
3	0.94	0.82530	0.76300	0.46774	0.64661
4	0.93	0.78165	0.70608	0.38022	0.60116
5	0.92	0.75094	0.68941	0.29584	0.58711
6	0.91	0.72532	0.66248	0.22148	0.56997

$$h^+_{VB} + H_2O \rightarrow \cdot OH + H^+ \quad (9)$$

$$e^-_{CB} + O_2 \rightarrow \cdot O_2^- \quad (10)$$

$$\cdot OH + MB \rightarrow CO_2 + H_2O \quad (11)$$

$$\cdot O_2^- + MB \rightarrow CO_2 + H_2O \quad (12)$$

Therefore, the active oxygen species $\cdot O_2^-$ generated during the irradiation process also contribute to dye degradation. $\cdot O_2^-$ can also react with photogenerated holes to form active ·OH radicals and peroxides, or react with hydrogen ion to form peroxides and release oxygen according to the following equations[17]:

$$\cdot O_2^- + 2H_2O + h^+_{VB} \rightarrow 2 \cdot OH + H_2O_2 \quad (13)$$

$$2 \cdot O_2^- + 2H^+ \rightarrow O_2 + H_2O_2 \quad (14)$$

The main active species is ·OH, while $\cdot O_2^-$ only partly contributes to MB degradation.[17] For the mechanism behind the photocatalytic degradation of MB in presence of α-Fe_2O_3 nanospindle powder, see Ref. 1.

CONCLUSIONS

Well-crystalline α-Fe_2O_3 nanospindles were synthesized using a simple solvothermal approach at temperature of 240°C and their morphological, crystalline, chemical composition, and photocatalytic properties evaluated by FESEM, TEM, XRD analysis, EDS, and UV–Vis measurements. The results showed that the α-Fe_2O_3 nanospindles possessed high absorption capacity in the ultraviolet light region. The hydrothermal treatment time had a strong effect on the recombination rate and adsorption capacity for methylene blue molecules. The α-Fe_2O_3 nanospindles treated for 48 h showed the highest photocatalytic activity and highest degradation in comparison with the other α-Fe_2O_3 samples, in particular achieving more than 78% photodegradation of MB in 6 h. In addition, analysis of the photocatalytic mechanism indicated that ·OH radicals play an essential role in the photodegradation system, and other active oxygen species also importantly contribute to the degradation of MB. We anticipate that such hydrothermally synthesized α-Fe_2O_3 nanospindle materials could be used as effective and promising photocatalysts for large-scale removal of methylene blue from wastewater and in various environmental applications. The photocatalytic performance for dye degradation could be improved by addition of proper amounts of Cu,[1] Eu,[23] CuO,[24] Ag,[25] Au,[26] or Sn.[27] Extensive research on controlling metal dopants in α-Fe_2O_3 nanospindles to achieve the best performance is currently ongoing.

ACKNOWLEDGMENTS

This work was supported by the Ministry of Education and Training of Vietnam via decision No. 5651/QĐ-BGDĐT-28/12/2018.

CONFLICT OF INTEREST

The authors declare that they have no conflicts of interest.

REFERENCES

1. N. Prasad and B. Karthikeyan, *Vacuum* 146, 501 (2017).
2. E. György, C. Logofatu, Á. Pérez del Pino, A. Datcu, O. Pascu, and R. Ivan, *Ceram. Int.* 44, 1826 (2018).
3. Y. Bessekhouad, D. Robert, and J.V. Weber, *J. Photochem. Photobiol. A Chem.* 157, 47 (2003).
4. A. Muthukrishnaraj, S. Vadivel, V.P. Kamalakannan, and N. Balasubramanian, *Mater. Res. Innov.* 19, 258 (2015).
5. S. Vadivel, M. Vanitha, A. Muthukrishnaraj, and N. Balasubramanian, *J. Water Process Eng.* 1, 17 (2014).
6. X. Qu, D. Xie, L. Cao, and F. Du, *Ceram. Int.* 40, 12647 (2014).
7. P. Sharma, R. Kumar, S. Chauhan, D. Singh, and M.S. Chauhan, *J. Nanosci. Nanotechnol.* 14, 6153 (2014).
8. X. Hu, J.C. Yu, J. Gong, Q. Li, and G. Li, *Adv. Mater.* 19, 2324 (2007).
9. L. Chen, S. Wu, D. Ma, A. Shang, and X. Li, *Nano Energy* 43, 177 (2018).
10. A. Rufus, N. Sreeju, V. Vilas, and D. Philip, *J. Mol. Liq.* 242, 537 (2017).
11. S. Zeng, K. Tang, T. Li, Z. Liang, D. Wang, Y. Wang, Y. Qi, and W. Zhou, *J. Phys. Chem. C* 112, 4836 (2008).
12. S. Zeng, K. Tang, T. Li, Z. Liang, D. Wang, Y. Wang, and W. Zhou, *J. Phys. Chem. C* 111, 10217 (2007).
13. J.-J. Wu, Y.-L. Lee, H.-H. Chiang, and D.K.-P. Wong, *J. Phys. Chem. B* 110, 18108 (2006).

14. S. Cao and Y. Zhu, *J. Phys. Chem. C* 112, 6253 (2008).
15. S.-N. Sun, C. Wei, Z.-Z. Zhu, Y.-L. Hou, S.S. Venkatraman, and Z.-C. Xu, *Chin. Phys. B* 23, 037503 (2014).
16. X. Xie, H. Yang, F. Zhang, L. Li, J. Ma, H. Jiao, and J. Zhang, *J. Alloys Compd.* 477, 90 (2009).
17. Y. Huang, D. Ding, M. Zhu, W. Meng, Y. Huang, F. Geng, J. Li, J. Lin, C. Tang, Z. Lei, Z. Zhang, and C. Zhi, *Sci. Technol. Adv. Mater.* 16, 014801 (2015).
18. J. Huang, M. Yang, C. Gu, M. Zhai, Y. Sun, and J. Liu, *Mater. Res. Bull.* 46, 1211 (2011).
19. L.-P. Zhu, N.-C. Bing, L.-L. Wang, H.-Y. Jin, G.-H. Liao, and L.-J. Wang, *Dalton Trans.* 41, 2959 (2012).
20. J. Lu, D. Chen, and X. Jiao, *J. Colloid Interface Sci.* 303, 437 (2006).
21. J. Qu, Y. Yu, C.-Y. Cao, and W.-G. Song, *Chem. A Eur. J.* 19, 11172 (2013).
22. W. Zhao, W. Ma, C. Chen, J. Zhao, and Z. Shuai, *J. Am. Chem. Soc.* 126, 4782 (2004).
23. C. Wang and L. Cao, *J. Rare Earths* 29, 727 (2011).
24. T. Arai, M. Yanagida, Y. Konishi, Y. Iwasaki, H. Sugihara, and K. Sayama, *Catal. Commun.* 9, 1254 (2008).
25. S. Sun, X. Chang, L. Dong, Y. Zhang, Z. Li, and Y. Qiu, *J. Solid State Chem.* 184, 2190 (2011).
26. E. Thimsen, F. Le Formal, M. Grätzel, and S.C. Warren, *Nano Lett.* 11, 35 (2011).
27. L. Yichuan, W. Gongming, W. Damon, Z. Jin, and L. Yat, *Nano Lett.* 11, 2119 (2011).